Influence of Turbulence on the Dynamo Threshold

J-P. Laval,[1] P. Blaineau,[2] N. Leprovost,[2] B. Dubrulle,[2] and F. Daviaud[2]

[1]Laboratoire de Mécanique de Lille, CNRS, UMR 8107, Boulevard Paul Langevin, F-59655 Villeneuve d'Ascq Cedex, France
[2]SPEC/DRECAM/DSM/CEA Saclay and CNRS, URA2464, F-91190 Gif sur Yvette Cedex, France

(Received 22 December 2005; published 23 May 2006)

We use direct and stochastic numerical simulations of the magnetohydrodynamic equations to explore the influence of turbulence on the dynamo threshold. In the spirit of the Kraichnan-Kazantsev model, we model the turbulence by a noise, with given amplitude, injection scale, and correlation time. The addition of a stochastic noise to the mean velocity significantly alters the dynamo threshold and increases it for any noise at large scale. For small-scale noise, the result depends on its correlation time and on the magnetic Prandtl number.

DOI: 10.1103/PhysRevLett.96.204503 PACS numbers: 47.27.−i, 47.65.−d, 91.25.Cw

The process of magnetic field generation through the movement of an electrically conducting medium is called a dynamo. In a fluid, the instability occurs when the magnetic Reynolds number Rm exceeds some critical value Rm_c. Despite their obvious relevance in natural objects, such as stars, planets, or galaxies, dynamos are not so easy to study or model. Computer resources limit the numerical study of dynamos to a range of either small Reynolds numbers Re (laminar dynamo), modest Rm and Re [1], or small $Pm = \mathrm{Rm}/\mathrm{Re}$ using large eddy simulation [2]. These difficulties explain the recent development of experiments involving liquid metals as a way to study the dynamo problem at large Reynolds number. In this case, the flow has a nonzero mean component and is fully turbulent. There is, in general, no exact analytical or numerical prediction regarding the dynamo threshold. However, prediction for the mean-flow action can be obtained in the "kinematic regime" where the magnetic field backreaction onto the flow is neglected (see, e.g., [3]). This approximation is very useful for optimization of experiments, so as to get the lowest threshold for dynamo action based only on the mean flow $\mathrm{Rm}_c^{\mathrm{MF}}$ [4–7]. It led to an accurate estimate of the measured dynamo threshold in the case of experiments, where the instantaneous velocity field is very close to its time average [8].

In contrast, unconstrained experiments with shear in the equatorial plane [7,9] are characterized by large velocity fluctuations, allowing the exploration of the influence of turbulence onto the mean-flow dynamo threshold. Theoretical predictions regarding this influence are scarce. Small velocity fluctuations produce little impact on the dynamo threshold [10]. Predictions for arbitrary fluctuation amplitudes can be reached by considering the turbulent dynamo as an instability (driven by the mean flow) in the presence of a multiplicative noise (turbulent fluctuations) [11]. In this context, fluctuations favor or impede the magnetic field growth depending on their intensity or correlation time. This observation is confirmed by recent numerical simulations of simple periodic flows with nonzero mean flow [12,13] showing that turbulence increases the dynamo threshold.

In the sequel we use direct and stochastic numerical simulation of the magnetohydrodynamic (MHD) equations to explore a possible explanation, linked with the existence of nonstationarity of the largest scales. We found that the addition of a stochastic noise to the mean velocity could significantly alter the dynamo threshold. When the noise is at small scale, the dynamo threshold is decreased, while it is increased for a large-scale noise. In the latter case, the noise correlation time plays a role, and reinforces this effect, as soon as it is larger than the mean eddy-turnover time. When interpreted within the Kraichnan-Kazantsev model of MHD flow, these results predict that large-scale (small-scale) turbulence inhibits (favors) dynamo action.

The MHD equations for incompressible fluids are

$$\partial_t \mathbf{u} + \mathbf{u}\cdot\nabla\mathbf{u} = -\nabla P + \nu\nabla^2\mathbf{u} + \mathbf{j}\times\mathbf{B} + f(t)\mathbf{v}^{\mathrm{TG}}, \quad (1a)$$

$$\partial_t \mathbf{B} = \nabla\times(\mathbf{u}\times\mathbf{B}) + \eta\nabla^2\mathbf{B}. \quad (1b)$$

Here, $\mathbf{u}$ is the velocity, $\mathbf{B}$ the Alfvén velocity, P the pressure, ν the viscosity, η the magnetic diffusivity, $\mathbf{j} = \nabla\times\mathbf{B}$, $\mathbf{v}^{\mathrm{TG}} = (\sin x\cos y\cos z, -\cos x\sin y\cos z, 0)$ the Taylor-Green (TG) vortex, and $f(t)$ is set by the condition that the (1, 1, 1) Fourier components of the velocity remain equal to $\mathbf{v}^{\mathrm{TG}}$. The equations are integrated on a triply periodic cubic domain using a pseudospectral method. The aliasing is removed by setting the solution of the 1/3 largest modes to zero. The time marching is done using a second-order finite difference scheme. An Adams-Bashforth scheme is used for the nonlinear terms while the dissipative terms are integrated exactly. The two control parameters are the Reynolds number $\mathrm{Re} = v_{\mathrm{rms}} l_{\mathrm{int}}/\nu$ and the magnetic Reynolds number $\mathrm{Rm} = v_{\mathrm{rms}} l_{\mathrm{int}}/\eta$, where $v_{\mathrm{rms}} = (1/3)\sqrt{2E} = (1/3)\sqrt{\langle u^2\rangle}$ is the (spatial) rms velocity based on the total kinetic energy $E = \int E(k)dk$ and $l_{\mathrm{int}} = (3\pi/4)E/\int kE(k)dk$ is the integral scale of the turbulent flow. Both v_{rms} and l_{int} fluctuate with time. Thus, viscosity and diffusivity are dynamically monitored so as to keep Re and Rm constant. We have checked that Re is a simple linear function of a nondynamical Reynolds number $\mathrm{Re}_{\mathrm{exp}} = v_{\max}\pi/\nu$ (usually used in experiments) based on maximum velocity and half the simulation box: $\mathrm{Re} = 7.41\mathrm{Re}_{\mathrm{exp}}$. Detailed comparison with previous results by Ponty *et al.* [2] is obtained by multiplying our Re and Rm by a factor $8/\sqrt{3}$. In the sequel, $\langle X\rangle$ ($\bar{X}$) refers to the spatial (time) average of X.

We ran typically four types of simulations: (i) direct numerical simulation (DNS)-MHD, where the full set of Eq. (1) is integrated at $5 \leq \mathrm{Re} \leq 100$ and $5 \leq \mathrm{Rm} \leq 50$ using resolutions up to 256^3; (ii) large eddy simulation (LES)-MHD at resolution 128^3, where the Lesieur-Chollet model of turbulence is used for the velocity Eq. (1a), allowing one to explore a case out of range of DNS [12], $\mathrm{Re} = 500$, $5 \leq \mathrm{Rm} \leq 100$; (iii) kinematic simulations; (iv) kinematic-stochastic (KS) simulations. In these last two cases, only the induction Eq. (1b) is integrated with $\mathbf{u}$ set to a given velocity field. In the kinematic case, it corresponds to the stationary velocity field $\bar{\mathbf{u}}(\mathrm{Re})$ obtained through time average of a stable solution of the Navier-Stokes equations with Taylor-Green forcing, at fixed Reynolds number. This procedure is complicated by hydrodynamic instabilities at low Reynolds number [14], imposing very long simulations (typically over 1000 s, i.e., 400 eddy-turnover times at $\mathrm{Re} = 46$) to ensure convergence towards an asymptotically stable solution. The average is then performed over several (typically 200) eddy-turnover times. In the KS case, the velocity field $\mathbf{u} = \bar{\mathbf{u}}(\mathrm{Re}) + \mathbf{v}'(k_I, \tau_c)$ is the sum of a time-averaged velocity field at a given Re and of an external Markovian Gaussian noise, with fixed amplitude v', correlation time τ_c, and typical scale k_I. In both kinematic simulations, the magnetic Reynolds number Rm is computed by using the rms velocity and integral scale of $\mathbf{u}$. In the deterministic case, this amounts to using $V_{\mathrm{rms}} = (1/3)\sqrt{\langle \bar{u}^2\rangle}$ and L_{int} the (spatial) rms velocity and integral scale of the time-averaged velocity field, like in optimization of dynamo experiments [4–7].

For each type of simulation, we fix Re (v', τ_c, and k_I, if needed), vary Rm, and monitor the time behavior of the magnetic energy $\langle B^2\rangle$ and the finite-time Lyapunov exponent $\Lambda = 0.5\partial_t\langle \ln(B^2)\rangle$, where the average is taken over the spatial domain. Four types of behaviors are typically observed [14]. (i) No dynamo: the magnetic energy decays, and the Lyapunov converges towards a finite negative value. (ii) Intermittent dynamo: the magnetic energy remains at a low level, with intermittent bursts of magnetic energy, and zero most probable value for the magnetic energy [11,15]. (iii) Mean-field dynamo: the magnetic energy grows with positive Lyapunov, and, in the DNS-MHD or LES-MHD, reaches a nonlinear saturated regime, with nonzero mean magnetic energy. (iv) Undecided state: with oscillation of the Lyapunov, so that no fit of the Lyapunov exponent can be obtained. From the values of the Lyapunov in the dynamo and the no-dynamo regime, one may derive the critical magnetic Reynolds number $\mathrm{Rm}_c(\mathrm{Re})$, solution of $\Lambda(\mathrm{Re}, \mathrm{Rm}_c) = 0$, through a standard interpolation procedure.

A summary of our exploration of the parameter space is provided in Fig. 1, for the nonstochastic simulations, where the only control parameters are Rm and Re. We did not detect any dynamo at $\mathrm{Re} = 2$. Decreasing Rm_c is observed in the window $2 < \mathrm{Re} < 4$, presumably caused by the almost 2D nature of the flow. Between $\mathrm{Re} = 4$ and $\mathrm{Re} = 10$, we observed heterocline dynamos, oscillating between a nondynamo and a dynamo state. The saturation state depends on Rm, going from stationary mean-field dynamo ($\mathrm{Rm} < 15$), to intermittent dynamo $15 < \mathrm{Rm} < 30$, then to turbulent mean-field dynamo ($\mathrm{Rm} > 30$). For $10 < \mathrm{Re} < 100$, we observed only turbulent mean-field dynamos, with critical magnetic Reynolds number for dynamo action in a turbulent flow $\mathrm{Rm}_c^{\mathrm{turb}}$ increasing with Re, in quantitative agreement with the result obtained in the same geometry, but with a different forcing (at constant force instead of constant velocity) [12]. Our LES-MHD simulation confirms the saturation of the dynamo threshold at large Reynolds number already observed in constant force simulations [12]. For the mean flow, we have detected two windows of dynamo actions, operating at $Pm < 1$ and $Pm > 1$: one, independent of Re, starting above $\mathrm{Rm}_c^{\mathrm{MF}} \approx 6$ and centered at $\mathrm{Rm} = 10$, with real Lyapunov (stationary dynamo); a second, occurring at larger Rm, with complex Lyapunov (oscillatory dynamo). One sees that $\mathrm{Rm}_c^{\mathrm{turb}}$ varies across these two windows and always exceeds $\mathrm{Rm}_c^{\mathrm{MF}}$. In the sequel, we show that the increase and saturation of $\mathrm{Rm}_c^{\mathrm{turb}}$ is not due to a crossing between the two dynamo modes, but to the influence of nonstationary large scales over $\mathrm{Rm}_c^{\mathrm{MF}}$.

To make an easier connection between DNS and KS simulations, we introduce a parameter that quantifies the noise intensity, $\delta = \overline{\langle u^2\rangle}/\langle \bar{u}^2\rangle$. This parameter depends on

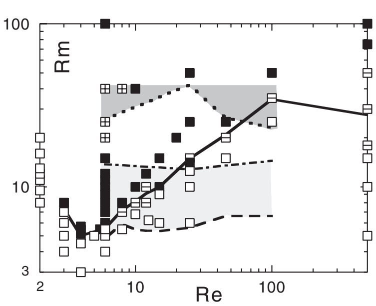

FIG. 1. Simulation parameter space. The square refer to DNS-MHD and LES-MHD simulations, and the shaded areas to explored windows of dynamo action for kinematic simulations with mean flow. □, no-dynamo case; ⊞, intermittent dynamo; ■, dynamo case; ⊟, undecided state; solid line, $\mathrm{Rm}_c^{\mathrm{turb}}$; dashed line, $\mathrm{Rm}_c^{\mathrm{MF}}$; dot-dashed line, end of the first kinematic dynamo window; dotted line, beginning of the second kinematic dynamo window.

the noise amplitude, as well as its correlation time and characteristic scale, and needs to be computed for each stochastic simulation. It can also be computed in the direct simulations and is found to depend on the Reynolds number, increasing from a value of 1 at low Reynolds number, to about 3 at the largest available Reynolds number [Fig. 2(a)]. Note that $\delta - 1$ is just the ratio of the kinetic energy of fluctuations onto the kinetic energy of the mean flow. In the sequel, the comparison between the KS and DNS-MHD simulations will therefore be made using δ as the control parameter. Another interesting information can be obtained from the energy spectrum of the velocity field, as one averages over longer and longer time scales [Fig. 2(b)]. One sees that during the first period of average (typically, a few eddy-turnover time, i.e., about 5 to 10 s), one mainly removes the fluctuations at largest scales, while the remaining average mostly removes small scales (over time scales of the order of 50 to 100 eddy-turnover times, i.e., 300 s).

In the sequel, we explore the influence of both type of fluctuations through the KS simulations, by considering noise at large ($k_I = 1$) and small scale ($k_I = 16$), with correlation time ranging from 0 to 50 s. Since the kinematic dynamo threshold is essentially constant for all values of the Reynolds number we explored, we first focus on the study of the case where the time-averaged field is fixed as $\bar{u}(\mathrm{Re} = 6)$ and vary the noise amplitude, characteristic scale, or correlation time, to explore their influence on the dynamo threshold. An example of our exploration of the parameter space is provided in Fig. 3, for different kinds of noise and $\bar{u}(\mathrm{Re} = 6)$. Note that by using our external noise, we are able to produce noise intensities comparable to experimental measurements ($\delta \sim 10$ at $\mathrm{Re} \sim 10^6$ for the von Kármán flow), and that are out of range of DNS. For low correlation time or injection scale, we are actually able to follow the deformation of the two windows of dynamo action. One sees that a noise does not destroy them, but rather distorts them. In the case where the noise is at large scale ($k_I = 1$), the windows are tilted upwards. In the case of small-scale noise ($k_I = 16$), the tilt is downwards for the first window at any τ_c, and for the second window at $\tau_c = 0$. For finite correlation time, the latter is bended upwards, in agreement with analytical results at large Pm [16].

In the sequel, we focus on the lowest dynamo window, the less computationally demanding. The influence of the noise onto the first dynamo threshold can be summarized by plotting the critical magnetic Reynolds numbers as a function of the noise intensity [Fig. 4(a)]. Large-scale (small-scale) noise tends to increase (decrease) the dynamo threshold. For small noise intensities, the correction $\mathrm{Rm}_c^{\mathrm{turb}} - \mathrm{Rm}_c^{\mathrm{MF}}$ is linear in $\delta - 1$, in agreement with the perturbative theory [10]. Furthermore, one sees that for small-scale noise, the decrease in the dynamo threshold is almost independent of the noise correlation time τ_c, while for the large-scale noise, the increase is proportional to τ_c at small τ_c. At $\tau_c \gtrsim 1$ s—one-third of the mean eddy-turnover time—all curves $\mathrm{Rm}_c(\delta)$ collapse onto the same curve. We have further investigated this behavior to understand its origin. Increasing δ first increases the flow turbulent viscosity $\overline{v_{\mathrm{rms}}}\,\overline{l_{\mathrm{int}}}$ with respect to its mean-flow value $V_{\mathrm{rms}} L_{\mathrm{int}}$. This effect can be corrected by considering $\mathrm{Rm}_c^* = \mathrm{Rm}_c V_{\mathrm{rms}} L_{\mathrm{int}} / \overline{v_{\mathrm{rms}}}\,\overline{l_{\mathrm{int}}}$. Second, an increase of δ produces an increase of the fluctuations of kinetic energy, quantified by $\delta_2 = \sqrt{\overline{\langle u^2 \rangle^2} - \overline{\langle u^2 \rangle}^2} / \overline{\langle u^2 \rangle}$. This last effect is more pronounced at $k_I = 1$ than at $k_I = 16$. It is amplified through increasing noise correlation time. We thus reanalyzed our data by plotting Rm_c^* as a function of δ_2 [Fig. 4(b)]. All results tend to collapse onto a single curve, independently of the noise injection scale and correlation time. This curve tends to a constant equal to $\mathrm{Rm}_c^{\mathrm{MF}}$ at low δ_2. This means that the magnetic diffusivity needed to achieve dynamo action in the mean flow is not affected by spatial velocity fluctuations. This is achieved for small-

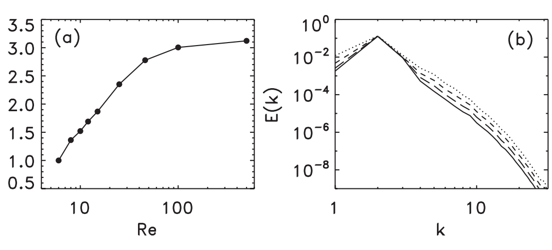

FIG. 2. (a) Noise intensity $\delta = \overline{\langle u^2 \rangle} / \langle \overline{u}^2 \rangle$, as a function of the Reynolds number in the DNS under the dynamo threshold. (b) Energy spectrum of the velocity field in the DNS, at Re = 46, for different average period T: dotted line, $T = 0$; short dashed line, $T = 75$ s; long dashed line, $T = 150$ s; solid line, $T = 300$ s.

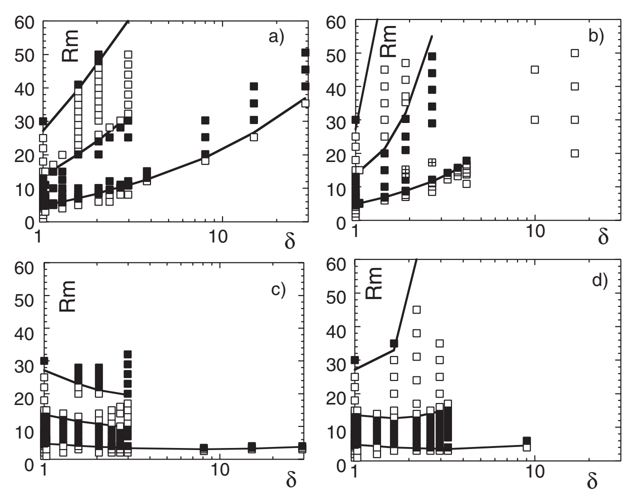

FIG. 3. Parameter space for noise at Re = 6 for different noise parameters: (a) $\tau_c = 0$, $k_I = 1$; (b) $\tau_c = 0.1$ s, $k_I = 1$; (c) $\tau_c = 0$, $k_I = 16$; (d) $\tau_c = 0.1$ s, $k_I = 16$. □, no-dynamo case; ⊞, undecided state; ■, dynamo case. The solid lines are zero-Lyapunov lines.

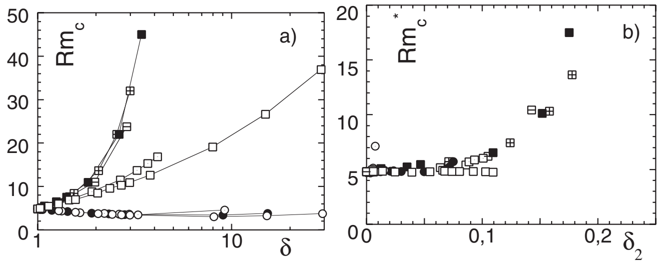

FIG. 4. Evolution of the dynamo threshold for KS simulations with $\bar{u}(\mathrm{Re} = 6)$. (a) Rm_c as a function of δ and (b) Rm_c^* as a function of δ_2 for different noise parameters. $k = 1$: □, $\tau_c = 0$; ⊡, $\tau_c = 0.1$ s; ⊟, $\tau_c = 1$ s; ⊞, $\tau_c = 8$ s; ■, $\tau_c = 50$ s. $k = 16$: ○, $\tau_c = 0$; ⊙, $\tau_c = 0.1$ s; ●, $\tau_c = 50$ s.

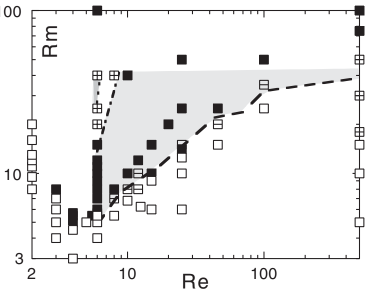

FIG. 5. Comparison between DNS and KS simulations with $\mathrm{Re} = 6$ with $k_I = 1$, $\tau_c \geq 1$ s. Same symbol meaning as in Fig. 1. Note the tiny dynamo window near $\mathrm{Re} = 6$, $\mathrm{Rm} = 40$.

scale noise, or large-scale noise with small correlation-time scale. In contrast, the curve diverges for δ_2 of the order of 0.2, meaning that time fluctuations of the kinetic energy superseding 20% of the total energy annihilate the dynamo. To check that our results are not affected by the choice of $\bar{u}$, we ran additional KS simulations with $\bar{u}$ computed at $\mathrm{Re} =$ 25, 46, and 100 for large-scale noise with correlation time $\tau_c \geq 1$ for the level of noise reached by the DNS at that Reynolds number. The obtained Rm_c were found to be within 10% (50%) the critical magnetic Reynolds numbers obtained at $\mathrm{Re} = 6$, for $\tau_c = 1$ ($\tau_c = 8$).

We now turn to detailed comparison of dynamo thresholds obtained in KS simulation at $k_I = 1$, for $\tau_c \gtrsim 1$ with the DNS-MHD case. In Fig. 5, we compare the two parameter spaces. One clearly sees that the noise-tilted first dynamo window coincides with the first mean-field dynamo window in the DNS-MHD, indicating that a large-scale noise is probably responsible from the increase of $\mathrm{Rm}_c^{\mathrm{turb}}$ with Re. Note that the noise intensity δ saturates past $\mathrm{Re} \sim 100$ [Fig. 2(a)], thereby explaining the saturation of $\mathrm{Rm}_c^{\mathrm{turb}}$ at large Re. A physical identification of this noise can be performed by visual inspection of the turbulent velocity field. One observes that the large-scale vortices generated by the Taylor-Green forcing are not exactly stationary, but wander slightly with time. A similar large-scale nonstationarity has been observed in the shear layer of von Kármán flows [17,18], with intensity corresponding to $\delta \sim 10$, and could thus be responsible for a significant increase of the dynamo threshold with respect to kinematic predictions.

Our work suggests that it might not be so easy to achieve turbulent dynamos in unconstrained geometries, with large-scale nonstationarity. In the experiments, a necessary ingredient for dynamo action could therefore be a monitoring of the large scale, so as to keep them as stationary as possible. In geo- and astrophysical flows, this role could be played by the Coriolis force. Our work also indicates that a well-chosen noise can be used in place of the actual turbulent velocity fluctuations to compute the dynamo threshold, at a much lower computational cost. In some sense, a kinematic-stochastic simulation can therefore be seen as a turbulent model and might be useful in the astro- or geophysical context.

We thank IDRIS, GDR Turbulence and Dynamo for support, and J-F. Pinton, Y. Ponty, A. Chiffaudel, and F. Plunian for discussions.

[1] G. A. Glatzmaier and P. H. Roberts, Nature (London) **377**, 203 (1995); C. Nore *et al.*, Phys. Plasmas **4**, 1 (1997); A. Schekochihin *et al.*, Phys. Rev. Lett. **92**, 054502 (2004); S. Boldyrev and F. Cattaneo, Phys. Rev. Lett. **92**, 144501 (2004).
[2] Y. Ponty *et al.*, Phys. Rev. Lett. **92**, 144503 (2004).
[3] M. L. Dudley and R. W. James, Proc. R. Soc. London **425**, 407 (1989).
[4] F. Stefani *et al.*, in *Transfer Phenomena in Magnetohydrodynamic and Electroconducting Flows*, edited by Ph. Marty *et al.* (Kluwer, Dordrecht, 1999), Vol. 31.
[5] L. Marié *et al.*, Eur. Phys. J. B **33**, 469 (2003).
[6] F. Ravelet *et al.*, Phys. Fluids **17**, 117104 (2005).
[7] C. B. Forest *et al.*, Magnetohydrodynamics **38**, 107 (2002).
[8] A. Gailitis *et al.*, Phys. Rev. Lett. **86**, 3024 (2001); R. Stieglitz and U. Müller, Phys. Fluids **13**, 561 (2001).
[9] N. L. Peffley, A. B. Cawthorne, and D. P. Lathrop, Phys. Rev. E **61**, 5287 (2000); M. Bourgoin *et al.*, Phys. Fluids **14**, 3046 (2002).
[10] S. Fauve and F. Pétrélis, *The Dynamo Effect*, Peyresq Lectures on Nonlinear Phenomena Vol. II, edited by J.-A. Sepulchre (World Scientific, Singapore, 2003).
[11] N. Leprovost and B. Dubrulle, Eur. Phys. J. B **44**, 395 (2005).
[12] Y. Ponty *et al.*, Phys. Rev. Lett. **94**, 164502 (2005); Y. Ponty *et al.*, physics/0601105.
[13] R. A. Bayliss *et al.*, physics/0602126.
[14] J.-P. Laval *et al.* (to be published).
[15] D. Sweet *et al.*, Phys. Plasmas **8**, 1944 (2001).
[16] A. Schekochihin and R. Kulsrud, Phys. Plasmas **8**, 4937 (2001).
[17] F. Ravelet, Ph.D. thesis, Ecole Polytechnique, 2005.
[18] R. Volk, Ph.D. thesis, ENS Lyon, 2005.